High glucose promotes hepatic fibrosis via miR-32/MTA3-mediated epithelial-to-mesenchymal transition

QIANG LI[1,2], ZHANGE LI[3], YUAN LIN[3], HUI CHE[1], YINGYING HU[4], XUJUAN KANG[3], YING ZHANG[3], LIHONG WANG[1] and YONG ZHANG[3,5]

[1]Department of Endocrinology, The Second Affiliated Hospital of Harbin Medical University, Harbin, Heilongjiang 150081; [2]Department of Gastroenterology, Heilongjiang Provincial Hospital, Harbin, Heilongjiang 150030; [3]Department of Pharmacology (The State-Province Key Laboratories of Biomedicine-Pharmaceutics of China, Key Laboratory of Cardiovascular Research, Ministry of Education), College of Pharmacy, Harbin Medical University, Harbin, Heilongjiang 150081; [4]Department of Pharmacy, The First Affiliated Hospital of Harbin Medical University; [5]Institute of Metabolic Disease, Heilongjiang Academy of Medical Science, Harbin, Heilongjiang 150086, P.R. China

Abstract. Hepatic fibrosis is characterized by the aberrant production and deposition of extracellular matrix (ECM) proteins. Growing evidence indicates that the epithelial-mesenchymal transition serves a crucial role in the progression of liver fibrogenesis. Although a subset of microRNAs (miRNAs or miRs) has recently been identified as essential regulators of the EMT gene expression, studies of the EMT in hyperglycemic-induced liver fibrosis are limited. In the current study, it was observed that high glucose-treated AML12 cells occurred EMT process, and miR-32 expression was markedly increased in the liver tissue of streptozotocin-induced diabetic rats and in high glucose-treated AML12 cells. Additionally, the contribution of the EMT to liver fibrosis by targeting metastasis-associated gene 3 (MTA3) under hyperglycemic conditions was suppressed by AMO-32. The results indicated that miR-32 and MTA3 may be considered as novel drug targets in the prevention and treatment of liver fibrosis under hyperglycemic conditions. These finding improves the understanding of the progression of liver fibrogenesis.

Correspondence to: Professor Lihong Wang, Department of Endocrinology, The Second Affiliated Hospital of Harbin Medical University, 246 Xuefu Road, Nangang, Harbin, Heilongjiang 150081, P.R. China
E-mail: nd6688@163.com

Professor Yong Zhang, Department of Pharmacology (The State-Province Key Laboratories of Biomedicine-Pharmaceutics of China, Key Laboratory of Cardiovascular Research, Ministry of Education), College of Pharmacy, Harbin Medical University, 157 Baojian Road, Nangang, Harbin, Heilongjang 150081, P.R. China
E-mail: hmuzhangyong@hotmail.com

Introduction

Type 2 diabetes mellitus (T2DM) is a metabolic disorder, and its prevalence significantly increases with age (1,2). Hyperglycemia is a prominent characteristic of T2DM, which results in secondary pathophysiological alterations in multiple organs, including the heart, lung and liver (3-5). Approximately 70% of patients with T2DM have fatty liver and exhibit a more severe course of liver fibrosis (6).

Hepatic fibrosis is characterized by the aberrant production and deposition of extracellular matrix (ECM) proteins, which leads to hepatic parenchyma and liver structure damage (7). Epithelial-to-mesenchymal transition (EMT) has been described as a principal mechanism for the deposition of ECM in liver, renal and pulmonary fibrosis injury models (8,9). Furthermore, adult hepatocytes serve a key role in the process of hepatic fibrogenesis via EMT (10,11). EMT is a dynamic biological process that induces epithelial cells to lose their typical properties and acquire the phenotypic traits of mesenchymal cell or fibroblast markers. EMT contributes to tissue repair, in addition to adversely causing organ fibrosis, including that of the kidney (12,13). Of the multiple stimuli involved in liver fibrosis, metastasis-associated protein MTA3 (MTA3) represses the transcription of Snail family transcriptional repressor 1 (Snail), an E-cadherin (E-cad) transcription activator by binding to its promoter region, although a Snail/MTA3 complex has not yet been observed (14,15). Further studies on the effects of MTA3 on EMT will assist in identifying novel therapeutic targets for liver fibrosis.

MicroRNAs (miRNAs/miRs) are endogenous, non-coding, single-stranded RNAs that mediate post transcriptional repression through complementary nucleotide sequence-specific binding to 3'-untranslated regions (3'-UTRs) of target mRNA, resulting in the degradation or inhibition of translation, and in some cases the destruction of the target mRNA (16,17). miRNAs participate in a wide range of pathophysiological processes, including cell proliferation, apoptosis, development and differentiation (18-21). Previous studies have demonstrated

that dysregulated miRNA expression and function are essential components in the development and progression of liver fibrosis. For example, the inhibition of miR-21 ameliorates liver fibrosis in schistosoma japonicum infections (22). Furthermore, miRNAs have been demonstrated to be involved in the EMT. For example, downregulation of miR-26a induces EMT by directly targeting high mobility group protein HMGI-C (4). Based on these observations, miRNAs may describe novel drug targets in liver fibrosis diagnosis, prevention and therapy.

Previous evidence has suggested that miR-32 regulates phosphatase and tensin homolog (PTEN) expression and serves a critical role in cell proliferation, migration and invasion in hepatocellular carcinoma and colorectal carcinoma (23,24). miR-32 negatively regulates mothers against decapentaplegic homology (Smad)7 expression and contributes to peribiliary fibrosis caused by *Clonorchis sinensis* infection (18). However, the detailed role of miR-32 in EMT, specifically in liver fibrosis, remains unknown. The present study was designed to investigate miR-32 expression under hyperglycemic conditions and evaluate its role in high glucose (HG)-induced liver fibrosis. The underlying mechanisms responsible for fibrosis and progression inhibition were assessed in the present study, and miR-32 and MTA3 were identified as potential therapeutic targets in liver fibrosis treatment.

Materials and methods

Establishment of a diabetic model. In total, 20 healthy 5-month-old male Wistar rats (180-220 g) were obtained from the Experimental Animal Center of Harbin Medical University (Harbin, China) and subjected to a 12/12 h light-dark cycle with standard animal room conditions (temperature, 22±1℃; humidity, 55±5%), with food and water available *ad libitum*. Rats were randomly divided into control and diabetic model (T2DM) groups. Non-diabetic rats were fed a standard diet. Rats with T2DM were gavaged with a high-fat diet (2 ml/day), which contained lard (20%), cholesterol (5%), sucrose (5%), glucose (5%) and salt (6%) emulsified in 20% Tween-80 with 30% propylene glycol in distilled water. After 2 weeks, diabetic rats were intraperitoneally injected with 35 mg/kg/day streptozotocin (STZ; Sigma-Aldrich; Merck KGaA, Darmstadt, Germany) in 0.1 M citrate buffer (pH 4.3) for 3 days, once a day. Following this, fasting blood glucose (FBG) levels were measured. FBG>16.7 nmol/l was considered to indicate a successfully established diabetic model.

Histopathological and morphometric analyses. Histopathological alterations and collagen distribution were evaluated by hematoxylin and eosin (H&E) and Masson's trichrome staining. The livers of rats in the control and T2DM groups were quickly excised and fixed in 4% paraformaldehyde for 24 h at 4℃ ad subsequently embedded in paraffin. The samples were cut into 5-μm-thick cross-sections and stained with H&E and Masson's trichrome reagent to assess the degree of fibrosis, as previously described (15,25). The degree of fibrosis was quantified with ImagePro Plus 6.0 software (Media Cybernetics, Inc., Rockville, MD, USA).

Cell culture and transfection. AML12 cells were purchased from the Type Culture Collection of the Chinese Academy

of Sciences (Shanghai, China) and cultured in a 1:1 mixture of Dulbecco's modified Eagle's medium/Ham's F-12 medium (HyClone; GE Healthcare Life Sciences, Logan, UT, USA), containing 5 μg/ml pre-mixed ITS (insulin, transferrin and sodium selenite; Sigma-Aldrich; Merck KGaA), 40 ng/ml dexamethasone (Sigma-Aldrich; Merck KGaA) and 10% fetal bovine serum (HyClone; GE Healthcare Life Sciences). The AML12 cells were maintained at 37℃ with 5% CO_2 and 95% air. When the culture reached 60% confluence, following culturing in serum-free medium for 6 h, the cells were transiently transfected with miRNA-32 mimics (5'-UAUUGCACAUUACUAAGUUGCA-3'), anti-miRNA oligonucleotide (AMO)-32 (5'-UGCAACUUAGUAAUGUGCAAUA-3') or negative control (5'-UUUGUACUACACAAAGUACUG-3') (NC; Guangzhou RiboBio Co., Ltd., Guangzhou, China) at a concentration of 100 nM. X-tremeGENE siRNA Transfection reagent (cat. no. 04476093001; Roche Diagnostics GmbH, Mannheim, Germany) was used as a transfection vehicle.

MTA3-overexpressing pcDNA3.1 (100 nM; IBSBIO, Shanghai, China) and the NC (100 nM; empty pcDNA3.1 plasmid) were transfected into AML12 cells using Lipofectamine® 2000 reagent (Invitrogen; Thermo Fisher Scientific, Inc., Waltham, MA, USA) according to the manufacturer's instructions.

Following incubation for 6 h, the culture medium was replaced with fresh medium, as described above, low glucose (LG; 1,000 mg/l) or HG (6,000 mg/l) medium for 24 h at 37℃. Protein and/or RNA was subsequently extracted from cells for further experimentation.

Identification of target gene. The potential target genes of miR-32 were predicted by TargetScanHuman Release 7.2 (http://www.targetscan.org/vert_72/), miRanda.org (http://miranda.org.uk/) and miRDB (http://www.mirdb.org/).

Luciferase reporter assays. Luciferase reporters containing the wild-type or mutated 3'-UTR of MTA3 were constructed by using psi-CHECK2 vectors (Promega Corporation, Madison, WI, USA). When the culture reached 90% confluence, the 293T (Cell Bank of Chinese Academy of Sciences, Shanghai, China) cells were seeded in a 24-well plate. When the 293T cells reached 60-70% confluence in a 24-well plate, the 3'-UTR luciferase vectors (100 mg) were co-transfected with miR-32 mimics, AMO-32 or NC using Lipofectamine® 2000 reagent, according to the manufacturer's protocol. *Renilla* luciferase reporters (10 ng) were used as an internal control. Following 48 h of transfection, luciferase activity was examined using the Dual-Luciferase Reporter assay system (Promega Corporation), according to the manufacturer's protocol.

RNA extraction and reverse transcription-quantitative polymerase chain reaction (RT-qPCR). Total RNA from rat liver tissues or from AML12 cells was lysed using 1 ml TRIzol® reagent (Invitrogen; Thermo Fisher Scientific, Inc.) according to the manufacturer's protocol. The extracted RNA was reverse transcribed into cDNA using a High-Capacity cDNA RT kit (cat. no. 4368814; Applied Biosystems; Thermo Fisher Scientific, Inc.) according to the manufacturer's protocol. The plates were incubated for 15 min at 16℃, 1 h at 37℃, 5 min at 85℃ and finally maintained at 4℃. A SYBR Green PCR Master Mix kit (cat. no. 4309155; Applied

Table I. Sequences of primers used for reverse transcription-quantitative polymerase chain reaction.

Gene	Species	Direction	Sequence (5'-3')
Collagen-1	Mouse	F	GAGCGGAGAGTACTGGATCG
		R	TACTCGAACGGGAATCCATC
	Rat	F	CAGCCCAAAGTGTGTGAGAA
		R	TGTGATGTTGGCCGTGTTAT
E-cadherin	Mouse	F	CAAGGACAGCCTTCTTTTCG
		R	AGCTCTGGGTTGGATTCAGA
	Rat	F	TCGGAGCATGTGAAGAACAG
		R	TGGCAGAACTGCATATTTCG
α-SMA	Mouse, rat	F	CCACCGCAAATGCTTCTAAGT
		R	GGCAGGAATGATTTGGAAAGG
Vimentin	Mouse	F	GATCAGCTCACCAACGACAA
		R	GGATTCCACTTTCCGTTCAA
	Rat	F	TCAGCTCACCAATGACAAGG
		R	GCTCCTGGATCTCTTCATCG
MTA3	Mouse	F	GGATTTGGCATATGTCCCTA
		R	ATATGGCTGAGCCGAAGAGA
	Rat	F	CATTGGTCTATGACCCCTCATTG
		R	GTCGATCCGTAAGTGGGCTAT
Snail	Mouse	F	CTTGTGTCTGCACGACCTGT
		R	CTTCACATCCGAGTGGGGTTT
	Rat	F	TGCACATCCGAAGCCACA
		R	TCTTCACATCCGAGTGGGTCTG
GAPDH	Mouse, rat	F	AAGAAGGTGGTGAAGCAGGC
		R	TCCACCACCCAGTTGCTGTA
miR-32	Mouse, rat	F	GCCACGCTATTGCACATTACTA
		R	TATCCAGTGCGTGTCGTGGAGT
U6	Mouse, rat	F	GCTTCGGCAGCACATATACTAAAAT
		R	CGCTTCACGAATTTGCGTGTCAT

F, forward; R, reverse; α-SMA, α-smooth muscle actin; MTA3, metastasis-associated protein MTA3; Snail, Snail family transcriptional repressor 1; miR-32, microRNA-32.

Biosystems; Thermo Fisher Scientific, Inc.) was used to quantify the relative levels of E-cad, α-smooth muscle actin (SMA), vimentin, MTA3, Snail and miR-32. GAPDH or U6 were used as an internal control. The cDNA samples were amplified in 96-well plates for 10 min at 95°C, followed by 40 cycles of 15 sec at 95°C, 30 sec at 60°C and 30 sec at 72°C and finally maintained at 4°C. The relative expression of the miRNA and mRNA were determined by the Cq ($2^{-\Delta\Delta Cq}$) method (26). qPCR was performed on a ABI 7500 FAST Real-Time PCR system (Applied Biosystems; Thermo Fisher Scientific, Inc.). The sequences of the primers used are presented in Table I.

Western blotting. Protein samples were obtained from liver tissues and AML12 cells using radioimmunoprecipitation assay (Beijing Solarbio Science & Technology Co., Ltd., Beijing, China) lysis buffer supplemented with protease inhibitors. Following centrifugation at 12,000 x g for 15 min at 4°C, the supernatant was collected and quantified using a bicinchoninic acid protein assay kit (Beyotime Institute of Biotechnology, Haimen, China). For the western blot analysis, 100 µg each protein sample was separated by SDS-PAGE (10% gels),

transferred to nitrocellulose membranes and blocked for 2 h with 5% non-fat milk at room temperature. Subsequently, the samples were incubated at 4°C overnight with primary antibodies against E-cad (1:1,000; cat. no. ab76055; Abcam, Cambridge, MA, USA), vimentin (1:1,000; cat. no. 7431; Cell Signaling Technology, Inc., Danvers, MA, USA), α-SMA (1:100; cat. no. ab7817; Abcam), MTA3 (1:1,000; cat. no. ab176346; Abcam), Snail (1:500; cat. no. ab82846; Abcam), GAPDH (1:1,000; cat. no. TA-08; ZhongShanJinQiao, Inc., Beijing, China) and collagen-1 (Col-1; 1:1,000, cat. no. ab34710; Abcam) in PBS. Membranes were incubated with a fluorescence-conjugated anti-rabbit immunoglobulin G secondary antibody (1:10,000; cat. no. 926-32211; LI-COR Biosciences, Lincoln, NE, USA) at room temperature for 1 h. The immunoreactivity were detected and quantified using an Odyssey Infrared Imaging System (LI-COR Biosciences) with Odyssey Software (LI-COR Biosciences; version 3.0).

Immunofluorescence staining. For immunofluorescence staining, AML12 cells were fixed with 4% paraformaldehyde in PBS for 30 min at room temperature and then

treated with 1% bovine serum albumin (cat. no. A-9647; Sigma-Aldrich; Merck KGaA) and 0.4% Triton X-100 (Beijing Solarbio Science & Technology Co., Ltd.) in PBS at room temperature for 2 h. Following blocking with 10% goat serum (cat. no. AR0009; Wuhan Boster Biological Technology Ltd., Wuhan, China), the cells were incubated with primary antibodies against E-cad (1:250; cat. no. ab76055; Abcam) and vimentin (1:100; cat. no. 7431; Cell Signaling Technology, Inc.) in PBS overnight at 4˚C. A secondary antibody conjugated with Alexa Fluor 594 (1:500; cat. no. A-11032; Invitrogen; Thermo Fisher Scientific, Inc.) in PBS was added and incubated with the cells for 1 h at 37˚C. Nuclei were stained using DAPI (1:500; Beyotime Institute of Biotechnology) for 20 min at room temperature. Immunofluorescence was examined using a confocal laser-scanning microscope (magnification, x200; Olympus Corporation, Tokyo, Japan).

Measurement of collagen content. Total collagen content was detected with a Biocolor Collagen Assay kit (cat. no. S1000; Biocolor Ltd., Carrickfergus, UK) according to the manufacturer's protocol. Briefly, lysates (100 μl) were collected from AML12 cells under HG conditions after 24 h. Sircol dye reagent (1 ml) binding to collagen was added to each sample and the solution was mixed at 4˚C for 30 min. Following centrifugation, 1 ml of the alkali reagent was added to each tube to dissolve the sediment. Subsequently, 200 μl of the sample was transferred to a each well of a 96-well plate to measure the absorbance at 540 nm. Total collagen (mg) was calculated using a linear calibration curve generated from standards and normalized to the total protein amount (mg) in each lysate.

Cell viability assay. A Cell Counting Kit-8 (CCK-8; Dojindo Molecular Technologies, Inc., Kumamoto, Japan) was used for the detection of cell viability. AML12 cells (60% confluence) were cultured with HG for 24 h. Subsequently, 10% CCK-8 solution was added to the cell culture medium and incubated for 1 h. The optical density was determined at 450 nm on a microplate reader and viability rates were calculated.

Statistical analysis. Data are presented as the mean ± standard error of the mean. Each experiment was replicated three times independently. Differences between groups were analyzed by one-way analysis of variance followed by Tukey's multiple-comparisons test. Comparisons between two groups were performed using Student's t-test. Statistical analysis was performed using GraphPad Prism version 5.0 (GraphPad Software, Inc., La Jolla, CA, USA). P<0.05 was considered to indicate a statistically significant difference.

Results

Epithelial-mesenchymal transition participates in liver fibrosis induced by hyperglycemia. A T2DM rat model was established, accompanied by hyperglycemia. Rats with T2DM exhibited significantly increased blood glucose levels, water intake, blood triglycerides (TG), total cholesterol (TC) and low-density lipoprotein (LDL), as well as decreased body weight and high-density lipoprotein (HDL; Table II). These markers indicated that the T2DM rat model was successfully established in the present study, similar to a previous study (4).

Table II. Rat characteristics in the control and diabetic groups, indicating the successfully established diabetic rat model.

Parameter	Control	Diabetic model
Food intake, g	20.9±0.1	22.3±0.2
Water intake, ml	68.2±1.0	122.0±0.4[a]
Body weight, g	288.2±8.6	226.1±3.2[a]
Blood glucose, mmHg	7.0±0.2	16.2±0.3[a]
TC, mmol/l	3.4±0.1	10.0±0.4[a]
TG, mmol/l	0.8±0.1	5.2±0.6[a]
LDL, mmol/l	1.7±0.1	4.2±0.1[a]
HDL, mmol/l	1.0±0.1	0.6±0.1[a]

[a]P<0.05 vs. control. TC, total cholesterol; TG, triglyceride; LDL, low-density lipoprotein; HDL, high-density lipoprotein.

It was observed that Col-1 protein and mRNA levels were significantly increased in the T2DM group (Fig. 1A and B). H&E and Masson's trichrome staining of the liver tissues revealed a broadened hepatic portal area, infiltrative inflammatory cells fibers spreading from the portal area and periportal fibrosis in the T2DM group (Fig. 1C). These findings indicated that hyperglycemia induced liver fibrosis, as previously described (6).

To evaluate whether EMT was involved in liver fibrosis, alterations in EMT marker expression were detected. E-cad, an epithelial marker, was markedly decreased. However, mesenchymal markers, including α-SMA and vimentin, increased in expression at the protein and mRNA level in rats with T2DM, compared with the control group (Fig. 1D and E). These results indicated that mesenchymal phenotypes may be involved in liver fibrosis induced by hyperglycemia.

HG induces the epithelial-mesenchymal transition in AML12 cells. To investigate the effects of HG on EMT in AML12 cells, Col-1, E-cad, α-SMA and vimentin protein (Fig. 2A) and mRNA (Fig. 2B) expression was evaluated. It was observed that Col-1, α-SMA and vimentin expression was significantly upregulated in the HG group, whereas E-cad expression was markedly downregulated, compared with the LG and control groups (Fig. 2A and B). Collagen content was significantly increased in HG-treated AML12 cells (Fig. S1). Normal AML12 cells exhibited a typical epithelial phenotype with a polygonal morphology and tight arrangement. However, exposure to HG for 24 h decreased E-cad (Fig. 2C) and increased vimentin (Fig. 2D) protein expression, compared with the control group, as determined by immunofluorescence. These alterations in E-cad and vimentin expression were in line with the aforementioned results. Hyperglycemic culture exposes cells to a hypertonic microenvironment (27), and cell viability under these conditions was assessed by CCK8 assays. As presented in Fig. S2, HG decreased cell viability compared with the control. These data suggested that HG may have induced EMT in AML12 cells.

miR-32 overexpression contributes to liver fibrosis progression and metastasis in AML12 cells. As the role of
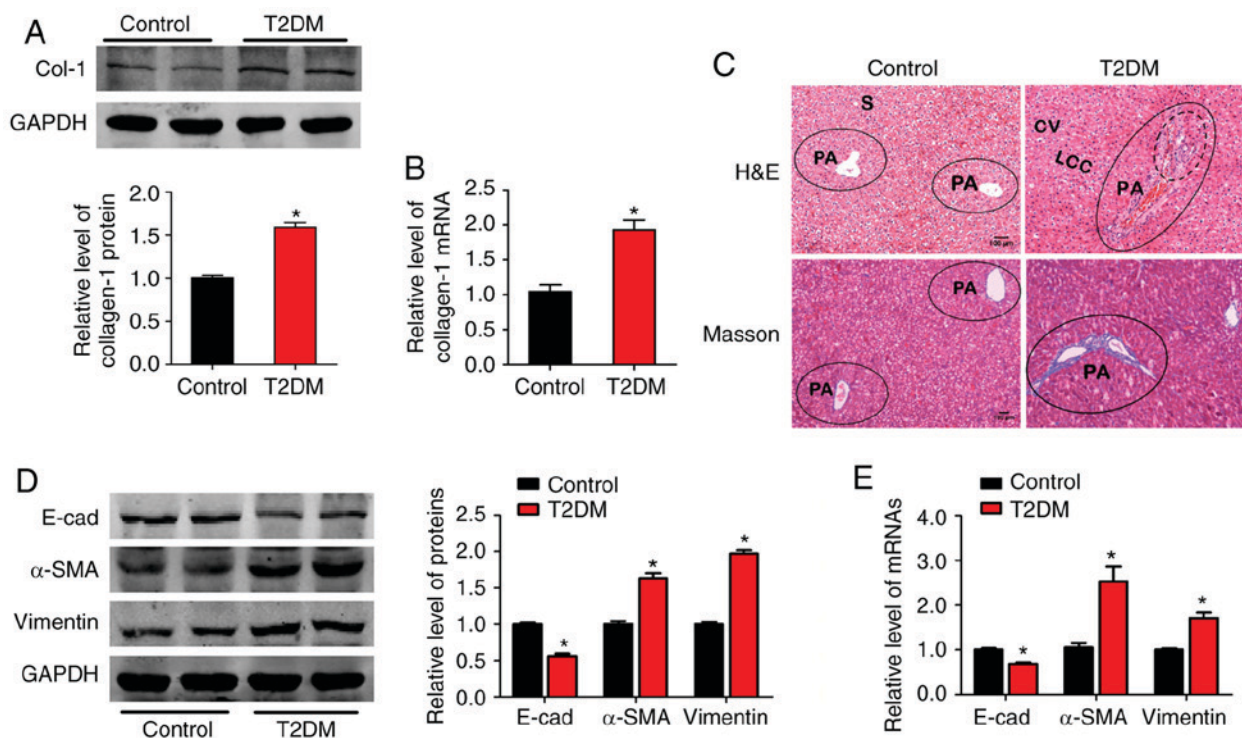
Figure 1. Epithelial-mesenchymal transition participates in liver fibrosis induced by hyperglycemia. (A) Relative Col-1 protein and (B) mRNA expression in liver tissues of the control and T2DM rats (n=5/group). (C) Histology was assessed by H&E staining and fibrillar collagen deposition was assessed by Masson's trichrome staining (magnification, x100). Dotted lines denote infiltration of inflammatory cells, solid lines and blue color indicates tissue fibrosis in the portal area (n=5/group). (D) Effects of hyperglycemia on expression of epithelial marker E-cad, mesenchymal markers α-SMA and vimentin by western blot and (E) reverse transcription-quantitative polymerase chain reaction (n=5/group). GAPDH was used as loading control. *P<0.05 vs. control group. Col-1, collagen-1; T2DM, type 2 diabetes mellitus; CV, central vein; LCC, hepatic cell cords; S, hepatic sinusoid; PA, portal area; E-cad, E-cadherin; α-SMA, α-smooth muscle actin; H&E, hematoxylin and eosin.
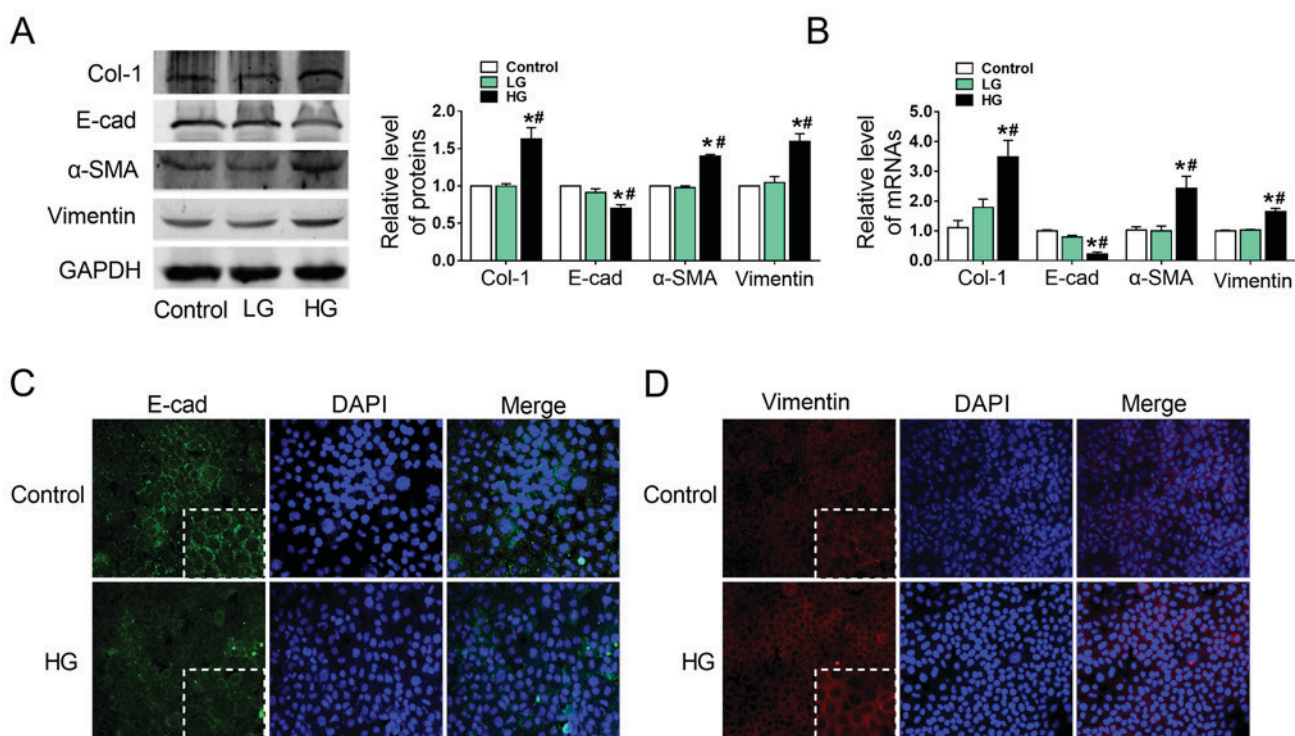

Figure 2. HG induces epithelial-mesenchymal transition in AML12 cells. (A) Alterations in Col-1, E-cad, α-SMA and vimentin protein expression in HG-treated AML12 cells was detected by western blotting, with representative blots on the left and relative quantification analysis on the right. (B) Relative mRNA expression of Col-1, E-cad, α-SMA and vimentin in HG-treated AML12 cells. GAPDH was used as an internal control. (C and D) Immunofluorescence images showing the location of EMT markers E-cad and vimentin in the control and HG-treated groups, with DAPI nuclear staining in blue, (C) E-cad in green and (D) vimentin in red (magnification, x200). *P<0.05 vs. control; #P<0.05 vs. LG groups. E-cad, E-cadherin; α-SMA, α-smooth muscle actin; Col-1, collagen-1; HG, high glucose (6,000 mg/l); LG, low glucose (1,000 mg/l).
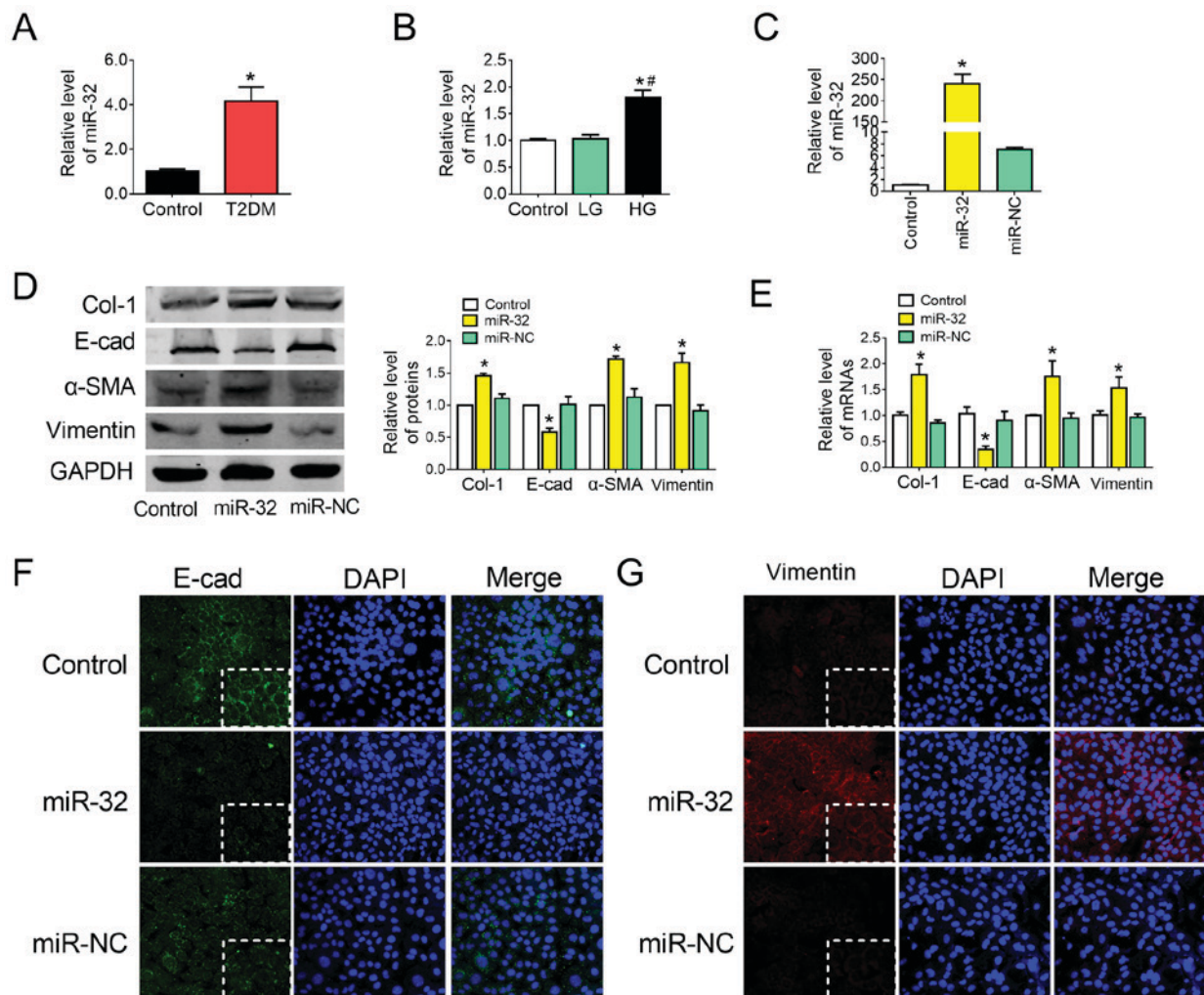
Figure 3. Overexpression of miR-32 contributes to liver fibrosis progression and metastasis in AML12 cells. (A) miR-32 levels were measured by RT-qPCR in the liver tissues of the control and rats with T2DM (n=4/group). (B) miR-32 expression was measured by RT-qPCR in HG-treated AML12 cells. *P<0.05 vs. control group; #P<0.05 vs. LG group. (C) miR-32 expression was measured by RT-qPCR in hepatocytes treated with miR-32 mimics (n=5/group). (D) Effect of miR-32 on Col-1, E-cad, α-SMA and vimentin protein expression, with representative blots on the left and the relative quantification analysis on the right (n=5/group). (E) Relative mRNA expression of Col-1, E-cad, α-SMA and vimentin was detected by RT-qPCR (n=5/group). GAPDH was used as an internal control. (F and G) Immunofluorescence images highlighting the location of EMT markers E-cad and vimentin, with DAPI nuclear staining in blue, (F) E-cad in green and (G) vimentin in red (magnification, x200). *P<0.05 vs. control group. E-cad, E-cadherin; α-SMA, α-smooth muscle actin; Col-1, collagen-1; miR-32, microRNA-32 mimic; miR-NC, microRNA-32 mimic NC; RT-qPCR, reverse transcription-quantitative polymerase chain reaction.

miR-32 and EMT in liver fibrosis remains unclear, miR-32 expression in liver tissue obtained from the T2DM group and in HG-treated AML12 cells was assessed by RT-qPCR. The results demonstrated that miR-32 was significantly upregulated in the liver tissue of the T2DM group (Fig. 3A) and in HG-treated AML12 cells (Fig. 3B), compared with the corresponding control groups. To investigate whether miR-32 was associated with EMT in liver fibrosis, cells were transfected with miR-32 mimics or AMO-32. Transfection efficiency was confirmed by RT-qPCR (Fig. 3C). It was observed that overexpression of miR-32 increased the protein (Fig. 3D) and mRNA (Fig. 3E) expression of Col-1, α-SMA and vimentin, and markedly downregulated E-cad expression (Fig. 3D and E). Additionally, collagen content was significantly increased following overexpression of miR-32 (Fig. S1). These results were supported and confirmed by immunofluorescent staining analysis for E-cad (Fig. 3F) and vimentin (Fig. 3G).

miR-32 knockdown inhibits liver fibrosis under HG conditions. It was investigated whether decreased miR-32 suppressed liver fibrosis by affecting EMT under hyperglycemic conditions. First, AMO-32 transfection efficiency was confirmed by RT-qPCR (Fig. 4A). It was observed that miR-32 inhibition decreased Col-1, α-SMA and vimentin at the protein (Fig. 4B) and mRNA (Fig. 4C) level in HG-treated AML12 cells. However, levels of E-cad were markedly up-regulated under miR-32 inhibition. In addition, a Sircol collagen assay suggested that collagen content was significantly decreased by miR-32 inhibition (Fig. S1). Similar results were observed in immunofluorescence staining results for E-cad (Fig. 4D) and vimentin (Fig. 4E). The results indicated that decreased miR-32 expression may inhibit liver fibrosis by affecting EMT in HG-treated AML12 cells.

Targeting of MTA3 by miR-32 has a direct functional effect on liver fibrosis under HG conditions. To explore the molecular mechanisms by which miR-32 functioned in the progression
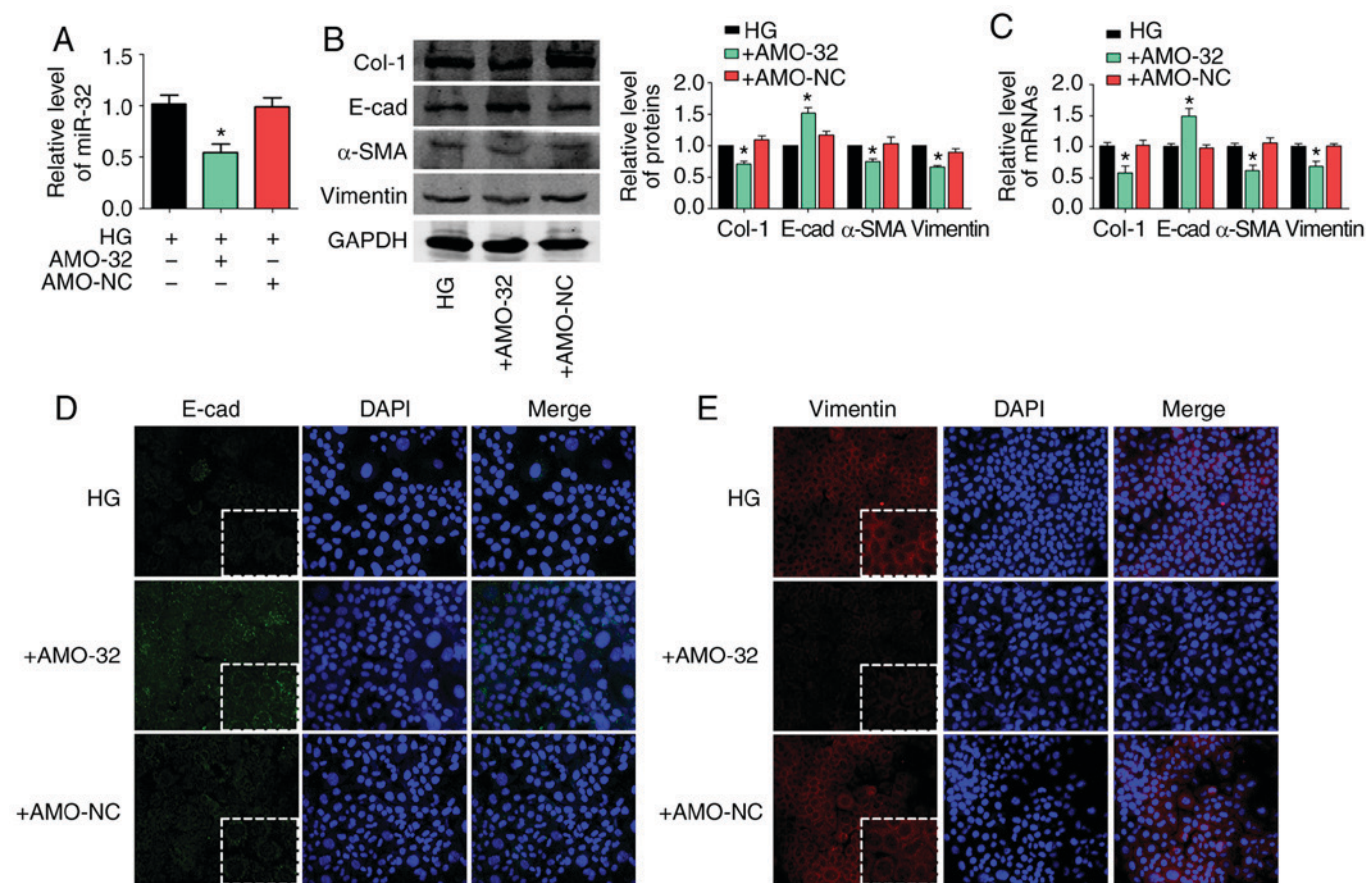
Figure 4. miR-32 knockdown inhibits liver fibrosis under HG conditions. (A) miR-32 expression was measured by RT-qPCR following transfection with AMO-32 under hyperglycemic conditions in AML12 cells (n=5/group). (B) Effects of miR-32 inhibition on Col-1, E-cad, α-SMA and vimentin protein expression in HG-treated AML12 cells, with representative blots on the left and the relative quantification analysis on the right (n=5/group). (C) Relative mRNA expression levels of Col-1, E-cad, α-SMA and vimentin were detected by RT-qPCR (n=5/group). GAPDH was used as an internal control. (D and E) Immunofluorescence images highlighting the location of EMT markers E-cad and vimentin, with DAPI nuclear staining in blue, (D) E-cad in green and (E) vimentin in red (magnification, x200). *P<0.05 vs. HG group. E-cad, E-cadherin; α-SMA, α-smooth muscle actin; Col-1, collagen-1; AMO-32, antisense inhibitor of miR-32; AMO-NC, negative control for AMO-32; HG: high glucose (6,000 mg/l); RT-qPCR, reverse transcription-quantitative polymerase chain reaction.

and metastasis of liver fibrosis, the TargetScan miRNA database was scanned to determine potential gene targets. Various targets were predicted, including MTA3, CXXC-type zinc finger protein 5 and bone morphogenetic protein 5. It was speculated that those involved in EMT may be relevant targets influencing the biological function of miR-32. Of these genes, MTA3 represses the transcription of Snail by binding to the promoter region of Snail. Snail contributes to the repression of E-cad transcription (28). It has been suggested that MTA3 is the major regulator and upstream protein in EMT.

To obtain further direct evidence that MTA3 was a target of miR-32, a binding site for miR-32 was identified on the MTA3 gene (Fig. 5A). In addition, luciferase reporter gene assays demonstrated that miR-32 significant suppressed luciferase activity, when using a vector carrying the wild-type 3'-UTR of MTA3, and a mutation in this binding site attenuated the action of miR-32 (Fig. 5B). Therefore, it was concluded that the inserted MTA3 fragment was a target of miR-32.

Based on the observations of the anti-fibrotic functions of decreased miR-32 expression and the bioinformatics analysis, the effects of miR-32 on MTA3 expression was investigated. MTA3 expression in the liver tissue and AML12 cells was assessed. Protein (Fig. 5C) and mRNA

(Fig. 5D) expression of MTA3 was significantly decreased in liver tissues of diabetic rats and in HG-treated AML12 cells, suggesting that MTA3 may be involved in hyperglycemia-induced liver fibrosis. Western blotting and RT-qPCR were performed to determine the effects of miR-32 on endogenous MTA3 protein and mRNA expression in AML12 cells. It was observed that the overexpression of miR-32 in AML12 cells markedly downregulated MTA3 protein and mRNA (Fig. 5E).

To confirm whether miR-32 regulated liver fibrosis through MTA3 changes in MTA3 protein and mRNA levels were assessed following miR-32 knockdown. In addition, EMT markers in MTA3 overexpressing HG-treated AML12 cells were evaluated. It was observed that miR-32 knockdown by AMO-32 increased MTA3 protein and mRNA levels compared with control and miR-NC cells (Fig. 5F). In addition, E-cad mRNA and protein levels were markedly increased by MTA3 overexpression. However, MTA3 overexpression decreased α-SMA and vimentin protein and mRNA levels at increased MTA3 levels in HG-treated AML12 cells (Fig. S3A and B). The transfection efficiency of MTA3-overexpressing plasmid was confirmed by western blotting (Fig. S3C). In conclusion, these findings indicated that miR-32 knockdown may ameliorate
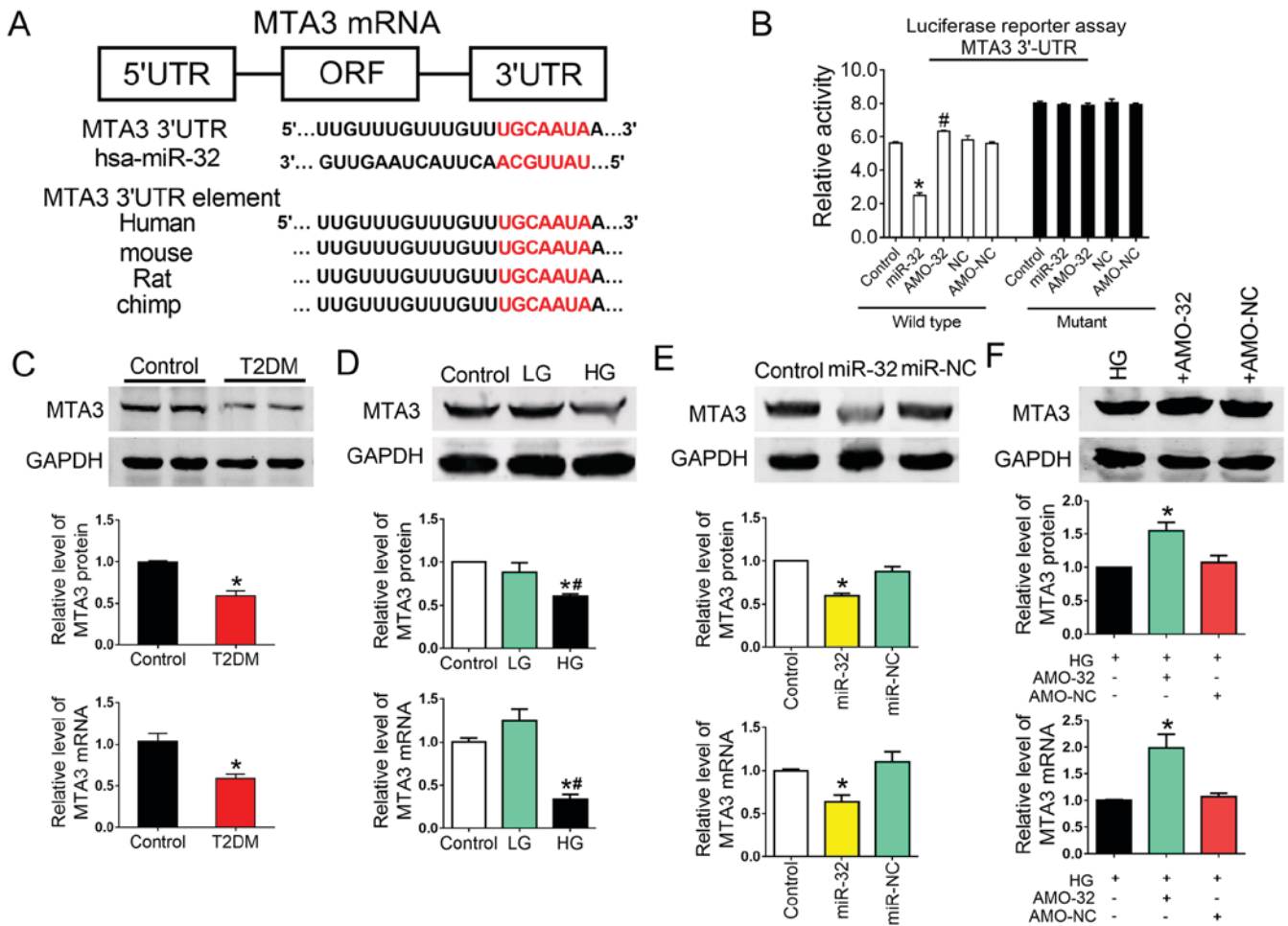
Figure 5. Targeting of MTA3 by miR-32 has a direct functional effect on liver fibrosis under HG conditions. (A) Sequence alignment highlighting complementary nucleotides between miR-32 and the 3'-UTR of MTA3; letters in red indicate matched bases. (B) Luciferase reporter gene assay exhibiting significantly reduced luciferase activities when using miR-32 mimics, and AMO-32 abolished the repressive effects. The mutated construct did not affect luciferase activity (n=5/group). *P<0.05 vs. control; #P<0.05 vs. miR-32. (C) MTA3 protein and mRNA expression in the livers of control and T2DM rats (n=5/group). *P<0.05 vs. control group. (D) MTA3 protein and mRNA expression in HG-treated AML12 cells (n=5/group). *P<0.05 vs. control group; #P<0.05 vs. LG group. (E) Effect of miR-32 on MTA3 expression in AML12 cells (n=5/group). *P<0.05 vs. control group. (F) MTA3 protein and mRNA expression in AML12 cells following transfection with AMO-32 under hyperglycemic conditions (n=5/group). *P<0.05 vs. HG group. miR-32, miR-32 mimic; T2DM, type 2 diabetes mellitus; AMO-32, antisense inhibitor of miR-32; AMO-NC, negative control for AMO-32; HG, high glucose (6,000 mg/l); 3'-UTR, 3'-untranslated region; MTA3, metastasis-associated protein MTA3.

liver fibrosis progression and metastasis via the regulation of MTA3 expression.

Downstream Snail acts as an indirect target of miR-32. Previous studies have suggested that Snail, an EMT-associated zinc finger transcription factor, is a transcriptional target of MTA3 (29,30). Therefore, it was hypothesized that Snail may be involved in the inhibition of liver fibrosis induced by decreased miR-32 expression. In the present study, Snail mRNA and protein expression was significantly increased in liver tissue of rats with T2DM and in HG-treated AML12 cells, compared with their respective controls (Fig. 6A and B). To further explore whether miR-32 indirectly regulated the participation of Snail in EMT, gain- and loss-of-function studies were performed. Treating the cells with a miR-32 mimic reduced Snail expression, as demonstrated by RT-qPCR. Furthermore, miR-32 overexpression decreased MTA3 protein expression in AML12 cells, and miR-32 inhibition by AMO-32 reduced Snail protein and mRNA in HG-treated AML12 cells (Fig. 6C and D).

Discussion

In the present study, it was observed that MTA3 was decreased in liver tissues of rats with T2DM and in HG-treated AML12 cells. A luciferase reporter assay demonstrated that miR-32 directly bound to the 3'-UTR of MTA3 and miR-32 overexpression in AML12 cells suppressed MTA3 expression. In addition, it was observed that Snail expression was significantly increased and E-cad was decreased in the liver tissue of rats with T2DM and in HG-treated AML12 cells. These results indicated that MTA3 may be involved in regulating Snail and E-cad expression, and could have an important role in EMT under hyperglycemic conditions.

Recently, miRNAs have emerged as important mediators of translational control and as regulators of a wide range of biological processes (31,32). Aberrantly expressed miRNAs are often implicated in the pathogenesis of specific diseases, including liver fibrosis (33,34). Various miRNAs have been reported as fibrosis promoters and potential prognostic
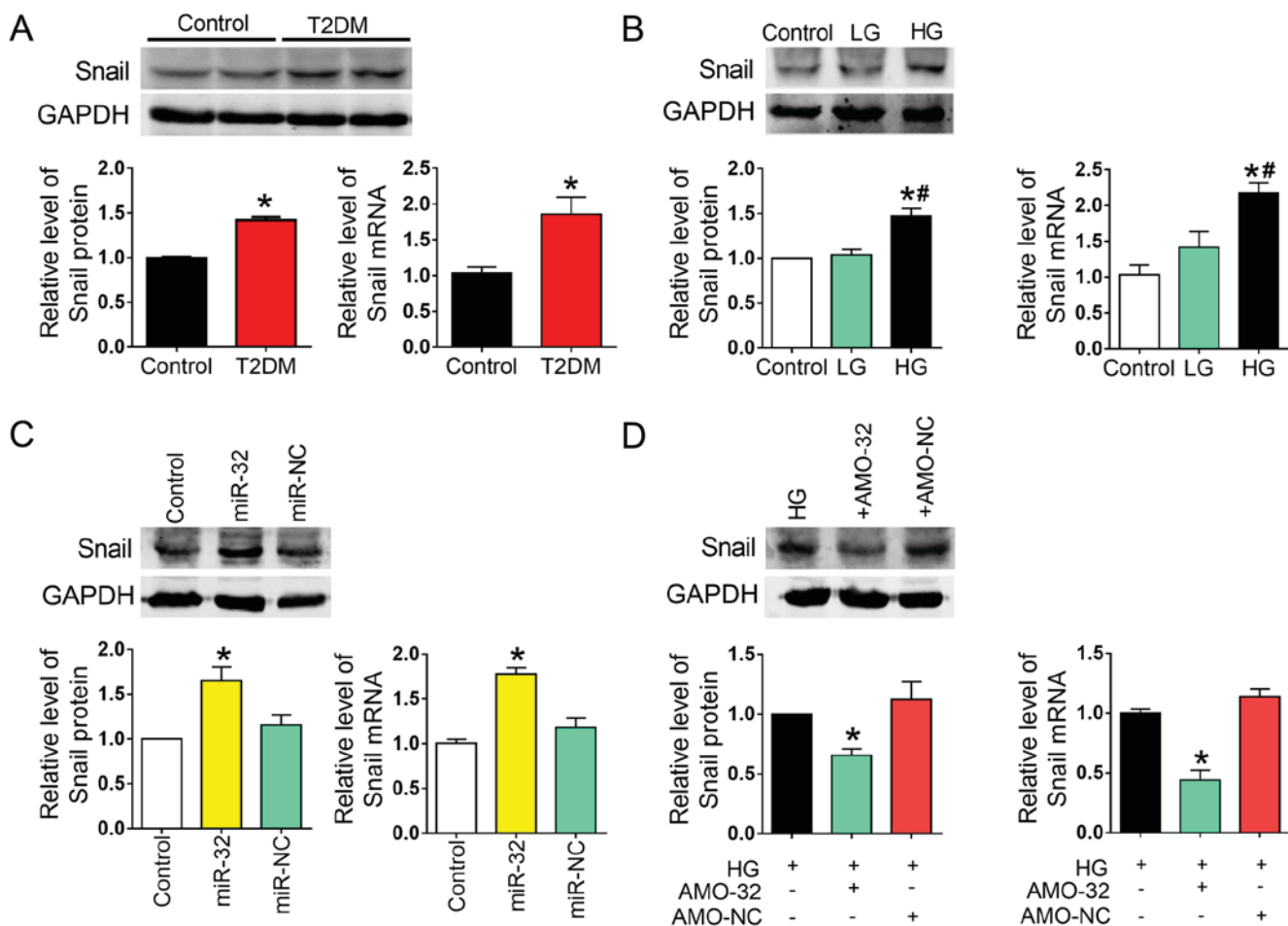
Figure 6. Downstream Snail acts as an indirect target of miR-32. (A) Relative protein and mRNA expression of Snail in liver tissues of the control and rats with T2DM (n=5/group). *P<0.05 vs. control group. (B) Relative protein and mRNA levels of Snail in AML12 cells treated with different concentrations of glucose (n=5/group). *P<0.05 vs. control group; #P<0.05 vs. LG group. (C) Relative protein and mRNA expression of Snail in the control, miR-32 and miR-NC groups (n=5/group). *P<0.05 vs. control group. (D) miR-32 knockdown resulted in decreased Snail protein and mRNA expression in HG-treated AML12 cells (n=5/group). *P<0.05 vs. HG group. T2DM, type 2 diabetes mellitus; HG, high glucose (6,000 mg/l); LG, low glucose (1,000 mg/l); miR-32, miR-32 mimic; AMO-32, antisense inhibitor of miR-32; AMO-NC, negative control for AMO-32; Snail, Snail family transcriptional repressor 1.

markers, including miR-29 and miR-155 (35,36); however, no direct evidence was available to support a role of miR-32 in liver fibrosis. In the current study, it was demonstrated that miR-32 expression was markedly increased in both streptozotocin-induced diabetic rats and HG-treated AML12 cells, indicating a potential role of miR-32 in liver fibrosis.

Previous studies have demonstrated that hyperglycemia in diabetic patients stimulates HSC activation and proliferation, and contributes to the development of hepatic fibrosis (37,38). EMT is an indispensable mechanism in embryogenesis, development and tissue remodeling, that contributes to the progression of organ fibrosis and cancer (39). Evidence suggested that several transcription factors, including overexpression of AmeloD resulted in E-cadherin suppression and dysregulation of interferon regulatory factor 5 regulated age-associated B cell formation by binding to promoter regions of involved genes (40,41). In particular, the transcriptional repressor Snail serves a critical role in suppressing E-cad transcription by binding to the CDH1 promoter (42,43). Additionally, studies have indicated that miRNAs, including the miR-200 family, regulate the EMT through overexpression-induced decreases in migration and invasion of pancreatic cancer cells by targeting the EMT-inducer zinc finger E-box binding homeobox 1 (44).

To illuminate the underlying molecular mechanisms by which miR-32 participates in liver fibrosis progression, various miRNA databases, including TargetScan, miRDB and miRanda, were utilized to validate MTA3 as a target gene for miR-32 that was conserved among various species. A previous study described that MTA3, histone deacetylase 1, nucleosome-stimulated ATPase Mi2 and the methyl-CpG binding protein-associated protein MBD3 form a Mi2/NuRD transcriptional repression complex, which inhibits Snail transcription by binding to its promoter region (14). Snail contributes to the repression of E-cad transcription; however, a Snail-MTA3 complex has not been identified thus far. Therefore, the current study investigated whether MTA3 was involved in regulating Snail and E-cad expression in diabetic rats and HG-treated AML12 cells.

In conclusion, the data from the current study provided the first evidence that miR-32 was dysregulated in HG-induced liver fibrosis and directly targeted MTA3. These findings support the existence of a novel pathway based on miR-32 and MTA3-Snail-induced EMT that may regulate liver fibrosis.

Consequently, the pathological loss of miR-32 may ameliorate hepatic fibrosis in T2DM and may provide a novel therapeutic approach for conditions associated with EMT.

Availability of data and materials

All data generated or analyzed during the present study are included in this published article.

Authors' contributions

YoZ, LW and QL participated in study design. QL, ZL, YL, HC, YH, XK and YiZ performed the experiments. QL, ZL, YL and YiZ analyzed the data. YoZ and LW contributed to the writing of the manuscript. All authors read and approved the final version of the manuscript.

Ethics approval and consent to participate

All animal experimental protocols were based on the regulations of the Ethics Committee of Harbin Medical University, conducted in accordance with the Laboratory Animal Management Regulations in China, and adhered to the Guide for the Care and Use of Laboratory Animals published by the National Institutes of Health (revised 2011).

Patient consent for publication

Not applicable.

Competing interests

The authors declare that they have no competing interests.

References

1. Gonçalves NP, Vægter CB, Andersen H, Østergaard L, Calcutt NA and Jensen TS: Schwann cell interactions with axons and microvessels in diabetic neuropathy. Nat Rev Neurol 13: 135-147, 2017.
2. Niu HS, Chao PC, Ku PM, Niu CS, Lee KS and Cheng JT: Amarogentin ameliorates diabetic disorders in animal models. Naunyn Schmiedebergs Arch Pharmacol 389: 1215-1223, 2016.
3. Li X, Du N, Zhang Q, Li J, Chen X, Liu X, Hu Y, Qin W, Shen N, Xu C, *et al*: MicroRNA-30d regulates cardiomyocyte pyroptosis by directly targeting foxo3a in diabetic cardiomyopathy. Cell Death Dis 5: e1479, 2014.
4. Liang H, Gu Y, Li T, Zhang Y, Huangfu L, Hu M, Zhao D, Chen Y, Liu S, Dong Y, *et al*: Integrated analyses identify the involvement of microRNA-26a in epithelial-mesenchymal transition during idiopathic pulmonary fibrosis. Cell Death Dis 5: e1238, 2014.
5. Zhuo J, Zeng Q, Cai D, Zeng X, Chen Y, Gan H, Huang X, Yao N, Huang D and Zhang C: Evaluation of type 2 diabetic mellitus animal models via interactions between insulin and mitogenacti-vated protein kinase signaling pathways induced by a high fat and sugar diet and streptozotocin. Mol Med Rep 17: 5132-5142, 2018.
6. Bril F and Cusi K: Management of nonalcoholic fatty liver disease in patients with type 2 diabetes: A call to action. Diabetes Care 40: 419-430, 2017.
7. Jiang H, Qin XJ, Li WP, Ma R, Wang T and Li ZQ: Effects of Shu Gan Jian Pi formula on rats with carbon tetrachloridein-duced liver fibrosis using serum metabonomics based on gas chromatographytime of flight mass spectrometry. Mol Med Rep 16: 3901-3909, 2017.
8. Li YK, Ma DX, Wang ZM, Hu XF, Li SL, Tian HZ, Wang MJ, Shu YW and Yang J: The glucagon-like peptide-1 (GLP-1) analog liraglutide attenuates renal fibrosis. Pharmacol Res 131: 102-111, 2018.
9. Li L, Li H, Zhang Z, Zheng J, Shi Y, Liu J, Cao Y, Yuan X and Chu Y: Recombinant truncated TGF-β receptor II attenuates carbon tetrachlorideinduced epithelialmesenchymal transition and liver fibrosis in rats. Mol Med Rep 17: 315-321, 2018.
10. Park JH, Yoon J, Lee KY and Park B: Effects of geniposide on hepatocytes undergoing epithelial-mesenchymal transition in hepatic fibrosis by targeting TGFβ/Smad and ERK-MAPK signaling pathways. Biochimie 113: 26-34, 2015.
11. Lee WR, Kim KH, An HJ, Kim JY, Lee SJ, Han SM, Pak SC and Park KK: Apamin inhibits hepatic fibrosis through suppression of transforming growth factor β1-induced hepatocyte epithelial-mesenchymal transition. Biochem Biophys Res Commun 450: 195-201, 2014.
12. Lovisa S, LeBleu VS, Tampe B, Sugimoto H, Vadnagara K, Carstens JL, Wu CC, Hagos Y, Burckhardt BC, Pentcheva-Hoang T, *et al*: Epithelial-to-mesenchymal transition induces cell cycle arrest and parenchymal damage in renal fibrosis. Nat Med 21: 998-1009, 2015.
13. Thiery JP, Acloque H, Huang RY and Nieto MA: Epithelial-mesenchymal transitions in development and disease. Cell 139: 871-890, 2009.
14. Fujita N, Jaye DL, Kajita M, Geigerman C, Moreno CS and Wade PA: MTA3, a Mi-2/NuRD complex subunit, regulates an invasive growth pathway in breast cancer. Cell 113: 207-219, 2003.
15. Qin W, Du N, Zhang L, Wu X, Hu Y, Li X, Shen N, Li Y, Yang B, Xu C, *et al*: Genistein alleviates pressure overload-induced cardiac dysfunction and interstitial fibrosis in mice. Br J Pharmacol 172: 5559-5572, 2015.
16. Bartel DP: MicroRNAs: Genomics, biogenesis, mechanism, and function. Cell 116: 281-297, 2004.
17. Du B, Wang X, Wu D, Wang T, Yang X, Wang J, Shi X, Chen L and Zhang W: MicroRNA expression profiles identify biomarkers for predicting the response to chemoradiotherapy in rectal cancer. Mol Med Rep 18: 1909-1916, 2018.
18. Huangfu L, Liang H, Wang G, Su X, Li L, Du Z, Hu M, Dong Y, Bai X, Liu T, *et al*: miR-183 regulates autophagy and apoptosis in colorectal cancer through targeting of UVRAG. Oncotarget 7: 4735-4745, 2016.
19. Zhang T, Hu Y, Ju J, Hou L, Li Z, Xiao D, Li Y, Yao J, Wang C, Zhang Y and Zhang L: Downregulation of miR-522 suppresses proliferation and metastasis of non-small cell lung cancer cells by directly targeting DENN/MADD domain containing 2D. Sci Rep 6: 19346, 2016.
20. Zhang Y, Qin W, Zhang L, Wu X, Du N, Hu Y, Li X, Shen N, Xiao D, Zhang H, *et al*: MicroRNA-26a prevents endothelial cell apoptosis by directly targeting TRPC6 in the setting of atherosclerosis. Sci Rep 5: 9401, 2015.
21. Yang B, Lin H, Xiao J, Lu Y, Luo X, Li B, Zhang Y, Xu C, Bai Y, Wang H, *et al*: The muscle-specific microRNA miR-1 regulates cardiac arrhythmogenic potential by targeting GJA1 and KCNJ2. Nat Med 13: 486-491, 2007.
22. Sombetzki M, Loebermann M and Reisinger EC: Vector-mediated microRNA-21 silencing ameliorates granulomatous liver fibrosis in Schistosoma japonicum infection. Hepatology 61: 1787-1789, 2015.
23. Wu W, Yang J, Feng X, Wang H, Ye S, Yang P, Tan W, Wei G and Zhou Y: MicroRNA-32 (miR-32) regulates phosphatase and tensin homologue (PTEN) expression and promotes growth, migration, and invasion in colorectal carcinoma cells. Mol Cancer 12: 30, 2013.

24. Yan SY, Chen MM, Li GM, Wang YQ and Fan JG: miR-32 induces cell proliferation, migration, and invasion in hepatocellular carcinoma by targeting PTEN. Tumour Biol 36: 4747-4755, 2015.
25. Zhang Y, Liu X, Bai X, Lin Y, Li Z, Fu J, Li M, Zhao T, Yang H, Xu R, et al: Melatonin prevents endothelial cell pyroptosis via regulation of long noncoding RNA MEG3/miR-223/NLRP3 axis. J Pineal Res 64: e12449, 2018.
26. Livak KJ and Schmittgen TD: Analysis of relative gene expression data using real-time quantitative PCR and the 2(-Delta Delta C(T)) method. Methods 25: 402-408, 2001.
27. Zálešák M, Blažíček P, Pancza D, Gablovský I, Štrbák V and Ravingerová T: Hyperosmotic environment blunts effectivity of ischemic preconditioning against ischemia-reperfusion injury and improves ischemic tolerance in non-preconditioned isolated rat hearts. Physiol Res 65: 1045-1051, 2016.
28. Kim NH, Cha YH, Lee J, Lee SH, Yang JH, Yun JS, Cho ES, Zhang X, Nam M, Kim N, et al: Snail reprograms glucose metabolism by repressing phosphofructokinase PFKP allowing cancer cell survival under metabolic stress. Nat Commun 8: 14374, 2017.
29. Dong H, Guo H, Xie L, Wang G, Zhong X, Khoury T, Tan D and Zhang H: The metastasis-associated gene MTA3, a component of the Mi-2/NuRD transcriptional repression complex, predicts prognosis of gastroesophageal junction adenocarcinoma. PLoS One 8: e62986, 2013.
30. Dhasarathy A, Kajita M and Wade PA: The transcription factor snail mediates epithelial to mesenchymal transitions by repression of estrogen receptor-alpha. Mol Endocrinol 21: 2907-2918, 2007.
31. Xiao D, Zhou T, Fu Y, Wang R, Zhang H, Li M, Lin Y, Li Z, Xu C, Yang B, et al: MicroRNA-17 impairs glucose metabolism in insulin-resistant skeletal muscle via repressing glucose transporter 4 expression. Eur J Pharmacol 838: 170-176, 2018.
32. Zhou T, Meng X, Che H, Shen N, Xiao D, Song X, Liang M, Fu X, Ju J, Li Y, et al: Regulation of insulin resistance by multiple miRNAs via targeting the GLUT4 signalling pathway. Cell Physiol Biochem 38: 2063-2078, 2016.
33. Tsay HC, Yuan Q, Balakrishnan A, Kaiser M, Möbus S, Kozdrowska E, Farid M, Tegtmeyer PK, Borst K, Vondran FWR, et al: Hepatocyte-specific suppression of microRNA-221-3p mitigates liver fibrosis. J Hepatol S0168-8278: 32635-32637, 2018.
34. Ji F, Wang K, Zhang Y, Mao XL, Huang Q, Wang J, Ye L and Li Y: miR-542-3p controls hepatic stellate cell activation and fibrosis via targeting BMP-7. J Cell Biochem 120: 4573-4581, 2019.
35. Bala S, Csak T, Saha B, Zatsiorsky J, Kodys K, Catalano D, Satishchandran A and Szabo G: The pro-inflammatory effects of miR-155 promote liver fibrosis and alcohol-induced steatohepatitis. J Hepatol 64: 1378-1387, 2016.
36. Roderburg C, Urban GW, Bettermann K, Vucur M, Zimmermann H, Schmidt S, Janssen J, Koppe C, Knolle P, Castoldi M, et al: Micro-RNA profiling reveals a role for miR-29 in human and murine liver fibrosis. Hepatology 53: 209-218, 2011.
37. Chen E, Cen Y, Lu D, Luo W and Jiang H: IL-22 inactivates hepatic stellate cells via downregulation of the TGF-β1/Notch signaling pathway. Mol Med Rep 17: 5449-5453, 2018.
38. Liu Z, Wang J, Xing W, Peng Y, Huang Y and Fan X: Role of DDAH/ADMA pathway in TGF-β1-mediated activation of hepatic stellate cells. Mol Med Rep 17: 2549-2556, 2018.
39. Chang J, Hu S, Wang W, Li Y, Zhi W, Lu S, Shi Q, Wang Y and Yang Y: Matrine inhibits prostate cancer via activation of the unfolded protein response/endoplasmic reticulum stress signaling and reversal of epithelial to mesenchymal transition. Mol Med Rep 18: 945-957, 2018.
40. He B, Chiba Y, Li H, de Vega S, Tanaka K, Yoshizaki K, Ishijima M, Yuasa K, Ishikawa M, Rhodes C, et al: Identification of the novel tooth-specific transcription factor AmeloD. J Dent Res 14: 22034518808254, 2018.
41. Manni M, Gupta S, Ricker E, Chinenov Y, Park SH, Shi M, Pannellini T, Jessberger R, Ivashkiv LB and Pernis AB: Regulation of age-associated B cells by IRF5 in systemic autoimmunity. Nat Immunol 19: 407-419, 2018.
42. Choi HJ, Park JH, Park M, Won HY, Joo HS, Lee CH, Lee JY and Kong G: UTX inhibits EMT-induced breast CSC properties by epigenetic repression of EMT genes in cooperation with LSD1 and HDAC1. EMBO Rep 16: 1288-1298, 2015.
43. Liu X, Ling M, Chen C, Luo F, Yang P, Wang D, Chen X, Xu H, Xue J, Yang Q, et al: Impaired autophagic flux and p62-mediated EMT are involved in arsenite-induced transformation of L-02 cells. Toxicol Appl Pharmacol 334: 75-87, 2017.
44. Wellner U, Schubert J, Burk UC, Schmalhofer O, Zhu F, Sonntag A, Waldvogel B, Vannier C, Darling D, zur Hausen A, et al: The EMT-activator ZEB1 promotes tumorigenicity by repressing stemness-inhibiting microRNAs. Nat Cell Biol 11: 1487-1495, 2009.